Korean J. Chem. Eng., **28**(7), 1497-1504 (2011)
DOI: 10.1007/s11814-010-0530-y

Modeling and simulation of hollow fiber CO_2 separation modules

Hyun Ju Jung*, Sang Hoon Han, Young Moo Lee**, and Yeong-Koo Yeo*,†**

*Department of Chemical Engineering, Hanyang University, Seoul 133-791, Korea
**WCU Department of Energy, Hanyang University, Seoul 133-791, Korea
(*Received 13 September 2010 • accepted 28 December 2010*)

Abstract−We developed two models for the CO_2 separation process by hollow-fiber membrane modules. The explicit model, which is based on mass balances for the separation modules, is compared with the multilayer perceptrons (MLP) back-propagation neural networks model. Experimental data obtained from single-stage module with recycle are used to validate the explicit model as well as to train the MLP neural model. The effectiveness of the model is demonstrated by little discrepancy between experimental data and computational results. The explicit model for the single-stage module can easily be extended to the multi(three)-stage module. Because of the lack of experimental data for multi-stage modules, computational data from the explicit model with and without recycle are used as training data set for the MLP neural model. We examined the effects of recycle on the recovery based on the results of numerical simulations, and could see that the predicting performance is improved by recycle for multi-stage module. From the results of numerical simulations, the proposed models can be effectively used in the analysis and operation of gas separation processes by hollow-fiber membrane modules.

Key words: Multi-stage Module, Multilayer Perceptrons Back-propagation Networks, Modeling of Separation Process, Carbon Dioxide, Hollow Fiber Membrane

INTRODUCTION

Separation of specific gases from exhaust gases may be accomplished by typical chemical engineering processes such as absorption, adsorption, cryogenic techniques and membrane methods. Among these separation methods, the use of polymeric membranes is becoming a standardized unit operation for various applications. One of the most promising applications using polymeric membranes is related to separation and recovery of CO_2 from exhaust gases. The cost of CO_2 separation occupies 70-80% of total cost required in CO_2 recovery and storage. Thus reduction of CO_2 separation cost makes the greatest contribution to improve economics of CO_2 treatment industry. Membrane separation processes are very attractive because of their lower energy consumption. In fact, membrane-based CO_2 separation has many advantages over other separation methods: 1) it is energy effective because phase transition is not involved; 2) operation and maintenance are simple because related facilities are compact and small; and 3) adjustment of operating conditions and scale-up are relatively easy [1]. Recently, a new membrane with high permeability (about 500 times as high as that of cellulose acetate membrane and about 300 times as high as that of polyimide membrane) was developed to enhance economics of CO_2 separation by membranes [2].

Use of models for the separation processes is common practice to evaluate the performance of CO_2 separation by membranes. In this work, we focus on the modeling of hollow-fiber membrane modules due to their widespread industrial use for membrane-based gas separation processes. In particular, models for several configurations of hollow-fiber membrane modules are investigated in this study. Modeling of CO_2 separation processes by membrane technology has received much attention in the past few decades. So far, explicit (or parametric) models represented in ordinary differential equations combined with algebraic equations have prevailed over empirical (or non-parametric) models [3,4]. Typical explicit models are based on mass and energy balances and fundamental knowledge of the process, while most of empirical models reported so far are based on neural networks. Noureddine et al. (1986) presented series solutions for co-current and counter-current flow hollow-fiber membrane separation processes [5]. Mathews et al. (1997) proposed models and numerical algorithms for radial cross flow, co-current and counter-current flow hollow-fiber membrane modules used in gas separation [6]. Results on the design and operation of multiple-stage hollow-fiber membrane separation processes were reported for CO_2 separation with recovery rate of 90% and mole fraction of 99% in the power generation plant using LNG feed [7]. They developed asymmetric hollow-fiber poly-isosulfone membrane modules. Song et al. [8,9] found that the partial pressure of CO_2 in the feed gas, the ratio of pressure between permeating side and membrane, and residence time of feed gas are considered to be the most significant factors affecting permeability of the membrane. They performed numerical analysis on the CO_2 separation characteristics for co-current and counter-current flow hollow-fiber poly-isosulfone membrane modules. Shahsavand and Chenar [10] proposed various neural network models for hollow fiber membrane processes. According to their results, both radial basis function and multilayer perceptron networks exhibit superior performance compared to models constructed by using conventional software tools.

This study presents both an explicit model and an empirical model for the CO_2 separation process by hollow-fiber membrane modules. The explicit model permits rapid solution of the governing differential mass and pressure distributions in hollow-fiber gas separation

†To whom correspondence should be addressed.
E-mail: ykyeo@hanyang.ac.kr

modules using a computational scheme that does not rely on commercial software and conventional numerical methods such as shooting techniques. The empirical model is based on back-propagation neural networks using multilayer perceptrons. Experimental data are used in training neural networks. Values of stage cuts can easily be identified for various desired mole fractions and recovery rates.

EXPERIMENTAL

Hollow fiber has larger membrane area in a unit volume compared with any other type of membranes and is most commonly used in membrane gas separation operations. Commercial hollow fiber membranes can provide less than 0.5 μm of effective thickness, which enables the membrane to show more than 6.7×10^{-10} mol/m^2·s·Pa of gas flux from 1 Barrer of membrane permeability. Thus, we can see that a material exhibiting 2000 Barrer of CO_2 permeability can be assumed to have more than 10^{-6} mol/m^2·s·Pa of CO_2 flux in a membrane module.

The precursor material of the hollow fiber membrane used in this work is hydroxyl-containing polyimide (HPI) which is prepared by the reaction of 4,4′-hexafluoroisopropylidene diphthalic anhydride (6FDA) and 2,2′-bis(3-amino-4-hydroxyphenyl) hexafluoropropane (bisAPAF) [2]. This HPI can be thermally converted into polybenzoxazole (PBO) by chain rearrangement, where the polymer chains can give rise to high free volume elements corresponding with high gas permeability.

Using dry-wet phase inversion method, hollow fiber membranes were prepared by extruding a dope solution composed of precursor polymer, N-methylpyrrolidinone (NMP) as a solvent and tetrahydrofuran (THF) as a volatile non-solvent. After the dope solution was spun from a spinneret connected to a gear pump, the hollow fiber membranes were wound to a cylindrical bobbin in an overflowing warm water bath until the residual solvents were fully eliminated by solvent exchange. The hollow fiber membrane was dried overnight at 150 °C, thermally rearranged in a muffled furnace at 450 °C and one hour, put in a membrane module made up of sustainable stainless steel (SUS), and finally sealed with epoxy adhesives.

Fig. 1 shows a schematic diagram for the membrane permeation test. Performance of the hollow fiber membrane module was measured in a temperature-controlled apparatus which can regulate the pressure and flow rate of each stream. For four streams (upstream in-let, upstream retentate, downstream sweep and downstream permeate), Kofloc 3660 and 3760 for mass flow controllers (MFCs) and meters (MFMs) (Kojima Instruments Inc., Kyoto, Japan) and Baratron 626A (1,000 torr) and 722A (20,000 torr) (MKS Instrument Corp., MA, USA) for pressure measurement were connected to a pressure and flow controller, MR-5000 (MJ Technics Co. Ltd., Incheon, Korea). Thus we could control the retentate stream rate which is to be used to calculate the stage-cut. The data were acquired continuously via RS-232 cable by Labview 7.1 software (National Instrument Corp., Austin, TX, USA). Each component was assembled with 1/4 inch SUS 316 tubes, tube fittings, 2-way and 3-way valves as shown in Fig. 1.

A gas chromatograph (GC-2010ATF, Shimadzu Corp., Kyoto, Japan) with an electrically controlled six-channel loop (Vici Valco Instruments Co. Inc., Houston, TX, USA) was introduced to analyze

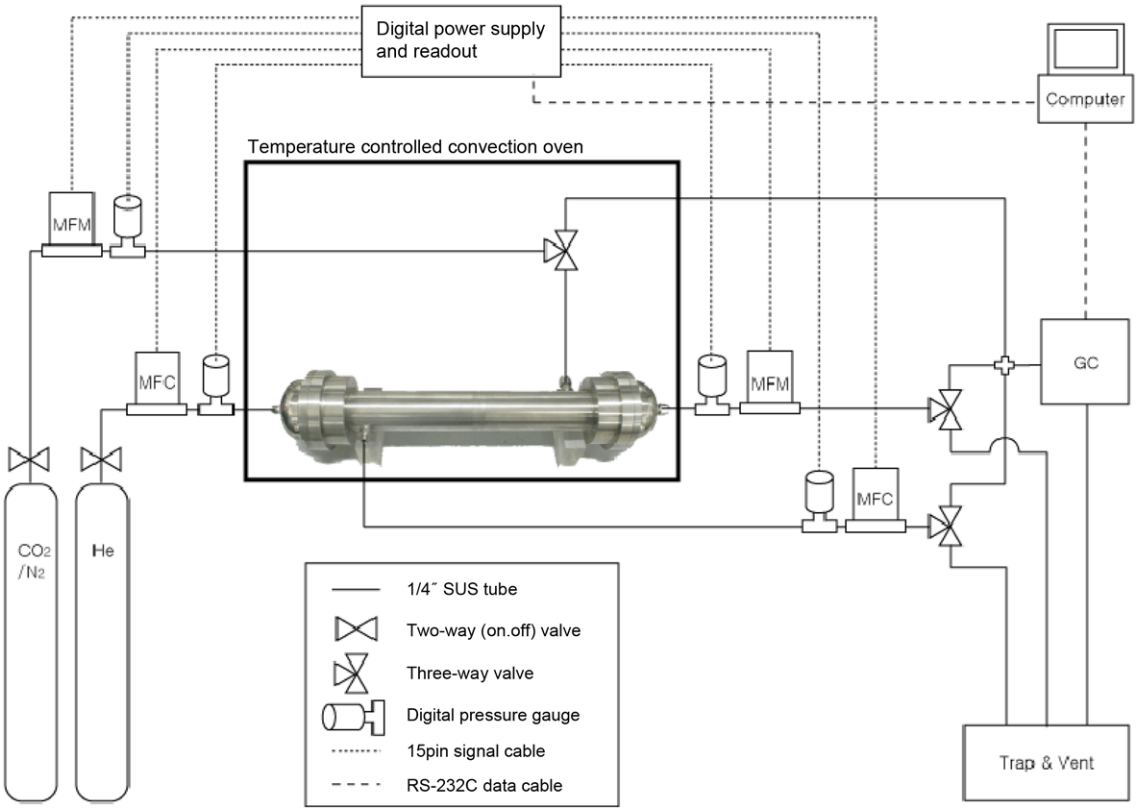

Fig. 1. Schematic diagram for the membrane permeation test.

the composition of each stream. The loop was opened in 30 sec and filled with the gas mixtures, then closed and swept into the detector by helium. Mixed gases with different compositions in in-let, retentate and permeate stream were separated in a Porapak Q packed column and detected in thermal conductive detector (TCD) detector every 3 minutes.

A gas mixture composed of 15 mol% of carbon dioxide and balance nitrogen was used as a simulated flue gas at upstream in-let stream, and high purity of helium (99.99+%) was used for sweep gas at downstream. In-let gas pressure was varied from 1 to 7 atm to make a difference in the pressure ratio and then optimized. At the retentate stream, gas flow rate was controlled to calculate the exact stage-cut, and pressure was measured to quantify a possible pressure drop compared to the in-let pressure. At the permeate stream, MFM rather than MFC was used so that the flow was not disturbed by the measurement instrument.

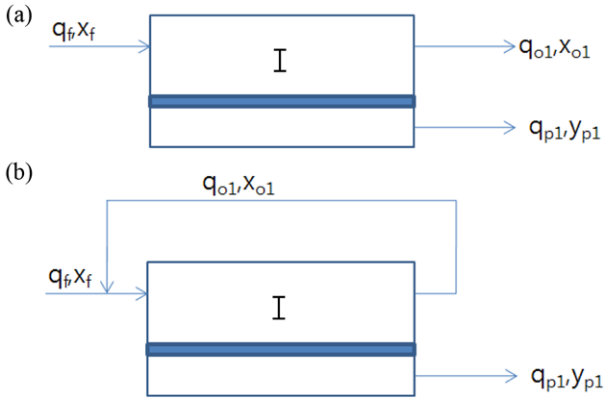

Fig. 3. Single-stage membrane separation module: without (a) and with (b) recycle.

EXPLICIT MODELS

Fig. 2 shows a single membrane separation module with complete mixing. The hollow-fiber bundle is sealed on both ends and is contained inside a high-pressure housing. Feed gas may be introduced on the bore of the hollow-fibers or on the shell side of the module. In the counter-current flow module, helium gas may be introduced in the opposite direction with feed gas. The helium gas may be introduced parallel to the feed gas in the co-current flow module. For the counter-current flow module, the difference in the driving force between the inlet and the outlet is negligible, while for the co-current flow module, the driving force decreases gradually from the inlet to the outlet [11,12]. For this reason, the counter-current flow module in general exhibits better separation performance as well as better operational flexibility, and only the counter-current flow module is considered in this study. The principal assumptions underpinning the model are:

- Shell side pressure change is negligible.
- The hollow-fibers consist of very thin membrane separation layers. All mass transfer resistance is confined to the separation membrane or the total membrane wall.
- There is no axial mixing of shell in the direction of bulk gas flow.
- The gas on the shell side of the hollow-fibers is in plug flow.
- The deformation of the hollow-fiber under pressure is negligible.
- All fibers have uniform inner and outer radius as well as a uniform thickness separation membrane.
- The membrane module is operated at steady-state.

1. Single-stage Module

Fig. 3 shows a single-stage module with and without recycle. Operation of the separator element at low recovery results in a minimal change in composition. In this case the complete-mixing model provides reasonable estimates of permeate purity. The overall material balance can be written as:

$$q_f = q_o + q_p \tag{1}$$

The stage-cut, θ, the fraction of feed permeated, is defined as:

$$\theta = \frac{q_p}{q_f} \tag{2}$$

The rate of diffusion or permeation of CO_2 is given by:

$$\frac{q_{CO_2}}{A_m} = \frac{q_p y_p}{A_m} = \left(\frac{P_{CO_2}'}{t}\right)(p_h x_o - p_l y_p) \tag{3}$$

Similar equations can be used for N_2 permeation.

$$\frac{q_{N_2}}{A_m} = \frac{q_p(1-y_p)}{A_m} = \left(\frac{P_{N_2}'}{t}\right)[p_h(1-x_o) - p_l(1-y_p)] \tag{4}$$

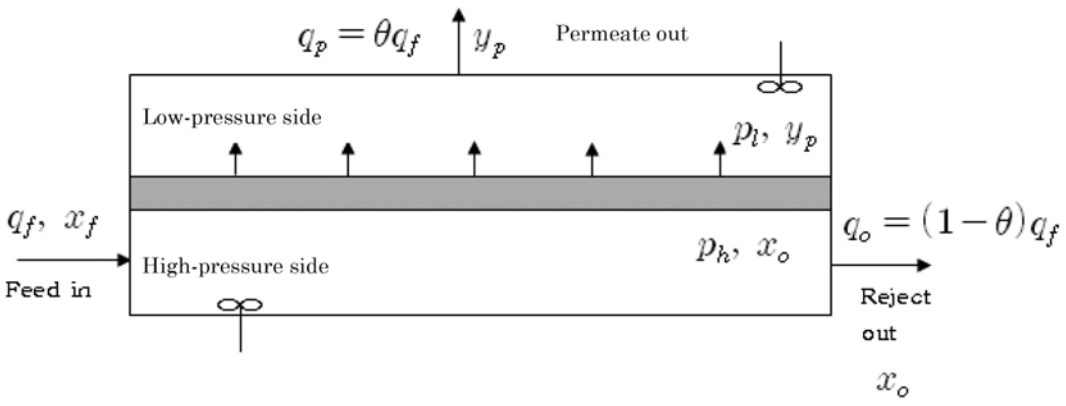

Fig. 2. A membrane separation module with complete mixing.

Division of Eq. (3) by Eq. (4) gives

$$\frac{y_p}{(1-y_p)} = \frac{\alpha^*[x_o-(p_l/p_h)y_p]}{(1-x_o)-(p_l/p_h)(1-y_p)} \tag{5}$$

This equation relates the permeate concentration y_p to the reject concentration x_o. The ideal separation factor α^* is defined by:

$$\alpha^* \equiv \frac{P_{CO_2}'}{P_{N_2}'} \tag{6}$$

The overall material balance on CO_2 can be represented as

$$q_f x_f = q_o x_o + q_p y_p \tag{7}$$

If we divide Eq. (7) by q_f and solve for the reject gas composition, we have

$$x_o = \frac{x_f-\theta y_p}{(1-\theta)} \text{ or } y_p = \frac{x_f-x_o(1-\theta)}{\theta} \tag{8}$$

Substituting $q_p=\theta q_f$ (from Eq. (2)) into Eq. (3) and solving for the membrane area, A_m, we get

$$A_m = \frac{\theta q_f y_p}{\left(\frac{P_{CO_2}'}{t}\right)(p_h x_o - p_l y_p)} \text{ or } y_p = \frac{x_f-x_o(1-\theta)}{\theta} \tag{9}$$

Normally values of x_f, θ, α^* and p_l/p_h are given and y_p, x_o, and A_m are to be determined. The main variable y_p is given by

$$y_p = \frac{-b_1+\sqrt{b_1^2-4a_1c_1}}{2a_1} \tag{10}$$

Where

$$a_1 = \theta + \frac{p_l}{p_h} - \frac{p_l}{p_h}\theta - \alpha^*\theta - \alpha^*\frac{p_l}{p_h} + \alpha^*\frac{p_l}{p_h}\theta$$

$$b_1 = 1-\theta-x_f-\frac{p_l}{p_h}+\frac{p_l}{p_h}\theta+\alpha^*\theta+\alpha^*\frac{p_l}{p_h}-\alpha^*\frac{p_l}{p_h}\theta+\alpha^* x_f$$

$$c_1 = -\alpha^* x_f$$

After solving for y_p, the values of x_o and A_m are calculated from Eqs. (8) and (9), respectively. The recovery ratio is defined by:

$$\text{recovery} \equiv \frac{q_p y_p}{q_f x_f} \tag{11}$$

2. Multi-stage Module

Modeling of a multi-stage separation system requires additional balance equations in addition to those for each stage. Fig. 4 shows a three-stage configuration of membrane separation module without and with recycle to the prior stage at each stage. The permeate gas from the previous stage becomes the feed gas to the next stage and the reject gas after 2nd-stage is recycled to the previous stage as the feed gas.

For a two-stage system, the total feed flow rate and the mole fraction of CO_2 to the 1st-stage are given by:

$$q_{f_1} = q_f + q_{O_2} \tag{12}$$

$$x_{f_1} = \frac{q_f x_f + q_{O_2} x_{O_2}}{q_f + q_{O_2}} \tag{13}$$

The total feed flow rate and the mole fraction of CO_2 to the 2nd-stage are given by:

$$q_{f_2} = q_{p_1} \tag{14}$$

$$x_{f_2} = y_{p_1} \tag{15}$$

For a three-stage system, the total feed flow rate and the mole fraction of CO_2 to the 1st-stage are given by:

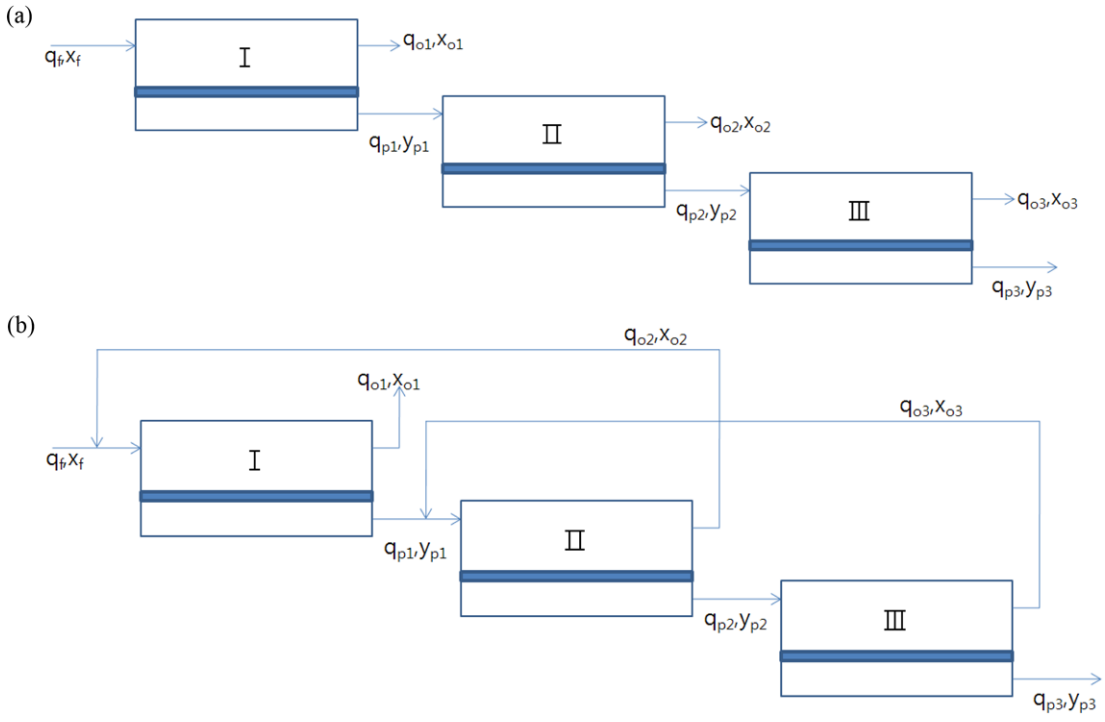

Fig. 4. 3-Stage membrane separation module: without (a) and with (b) recycle.

$$q_{f_1} = q_f + q_{O_2} \tag{16}$$

$$x_{f_1} = \frac{q_f x_f + q_{O_2} x_{O_2}}{q_f + q_{O_2}} \tag{17}$$

The total feed flow rate and the mole fraction of CO_2 to the 2^{nd}-stage are given by:

$$q_{f_2} = q_{p_1} + q_{O_3} \tag{18}$$

$$x_{f_1} = \frac{q_{p_1} x_{p_1} + q_{O_3} x_{O_3}}{q_{p_1} + q_{O_3}} \tag{19}$$

The total feed flow rate and the mole fraction of CO_2 to the 3^{rd}-stage are given by:

$$q_{f_3} = q_{p_2} \tag{20}$$

$$x_{f_3} = y_{p_2} \tag{21}$$

NEURAL NETWORK MODELING

Neural network modeling of membrane separation processes has been an active research subject in the past few years. The main advantage of neural network modeling is the successful recovery of the true underlying multidimensional hyper-surface hidden in a bunch of noisy measured data for various membrane separation processes. Feedforward neural networks are well-known examples among various neural network strategies. In the feedforward network, the neurons are generally grouped into layers which include input, hidden and output layer. Signals flow from the input layer through to the output layer via unidirectional connections, the neurons being connected from one layer to the next, but not within the same layer. Examples of feedforward networks include the multi-layer perceptron (MLP) [13], the learning vector quantization (LVQ) network [14] and the group-method of data handling (GMDH) network [15]. Feedforward networks can most naturally perform static mappings between an input space and an output space: the output at a given instant is a function only of the input at that instant.

In a recurrent network, the outputs of some neurons are fed to the same neurons or to neurons in preceding layers. Thus, signals can flow in both forward and backward directions. Examples of recurrent networks include Hopfield network [16], Elman network [17] and Jordan network [18]. Recurrent networks have a dynamic memory: their outputs at a given instant reflect the current input as well as previous inputs and outputs.

Neural networks are trained by two main types of learning algorithms: supervised and unsupervised learning algorithms. In addition, there exists a third type, reinforcement learning, which can be regarded as a special form of supervised learning. A supervised learning algorithm adjusts the strengths or weights of the inter-neuron connections according to the difference between the desired or target outputs and networks outputs. Examples of supervised learning algorithms include the delta rule [19], the generalized delta rule or back-propagation algorithm [13] and the LVQ algorithm [14]. Unsupervised learning algorithms do not require the desired outputs to be known. During training, only input patterns are presented to the neural network which automatically adapts the weights of its connections to cluster the input patterns into groups with similar features. Examples of unsupervised learning algorithms include the Kohonenand [14] Carpenter-Grossberg adaptive resonance theory (ART) [20] competitive learning algorithms. Reinforcement learning is a special case of supervised learning. Instead of using a teacher to give target outputs, a reinforcement learning algorithm employs a critic only to evaluate the goodness of the neural network output corresponding to a given input. An example of a reinforcement learning algorithm is the genetic algorithm (GA) [21,22].

The basic element of a multi-layer perceptron (MLP) neural network is the artificial neuron which performs a simple mathematical operation on its inputs. The input of the neuron consists of the variables $x_1, \ldots, x_p$ and a threshold (or bias) term. Each of the input values is multiplied by a weight, ω_i, after which the results are added with the bias term. A known activation function, φ, performs a pre-specified (nonlinear) mathematical operation on the results. MLP networks [10] may consist of many neurons ordered in layers. The neurons in the hidden layers do the actual processing, while the neurons in the input and output layer merely distribute and collect the signals. Although many hidden layers can be used, one hidden layer networks are more popular for practical applications due to their simple structures. The MLP network is trained by adapting the synaptic weights using a back-propagation technique or any other optimization procedure. During training phase, the network output is compared with a desired output. The error between these two signals is used to adapt the weights. This rate of adaptation may be controlled by a learning rate. A high learning rate will make the network adapt its weights quickly, but will make it potentially unstable. Setting the learning rate to zero will make the network keep its weights constant. The steepest descent optimization technique with constant step length parameters (η) is employed in this article. Additional linear weights are used in this work to accelerate the network convergence. The optimal values of these linear parameters are updated after each evaluation of the back-propagation method by using the following equation:

$$(\phi^T \phi)\underline{\alpha} = \phi^T \underline{y} \tag{22}$$

where $\phi_{ij} = \varphi(z_{i,j})$, i=1, …, N and j=1, …, M and y is the N×1 vector of measured values. The parameters N and M represent number of training data and number of neurons, respectively. In this work the feedforward back-propagation functions of MATLAB toolbox were used in the training and simulations. In the model one hidden layer was used. It was found that increasing the number of hidden layers deteriorates the estimation performance. 20 neurons were employed in the hidden layer. The number of neurons does not affect significantly the predicting performance. In some sense, the choice of the number of neurons in the hidden layer may be a trial-and-error procedure. From several trials we found that 20 neurons give the best performance.

RESULTS AND DISCUSSION

In experiments, the surface of the porous support was treated with the membrane the properties of which are given in Table 1 which also shows experimental conditions and parameters used in experiments and simulations. A gas mixture composed of 15 mol% of carbon dioxide and balanced nitrogen was used as a simulated flue gas at upstream in-let stream, and high purity of helium (99.99+%) was used for sweep gas at downstream (see Fig. 1). In-let gas pres-

Table 1. Conditions and parameters used in experiments and numerical simulations

Type	Value
p_f	1.4 [bar]=140000 [Pa]
p_l	0.2 [bar]=20000 [Pa]
α^*	25 [-]
x_f	0.15 [-]
q_f	500 [m^3/hr]=80357142.86 [mol/hr]
T	25 [°C]=298.15 [K]
R	8.314 [J/mol·K]
(P_{CO_2}'/t)	10^{-6} [mol/m^2·s·Pa]=3.6×10^{-3} [mol/m^2·hr·Pa]

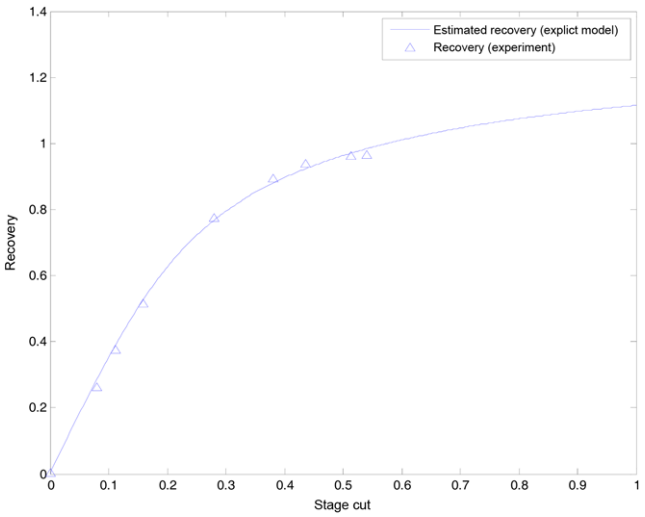

Fig. 5. Experimental data compared with results of numerical simulations.

sure was varied from 1-7 atm to make a difference in the pressure ratio and then optimized. Gas flow rate of the retentate stream was controlled to calculate the exact stage-cut, and pressure was measured to quantify a possible pressure drop compared to the in-let pressure. The selectivity and the area of the membrane are 25 and 1.813 m^2, respectively.

Experimental results are shown in Fig. 5 as well as calculation results obtained from the explicit model. In the calculations some modification is required for the porous supporting material used in experiments. The approach adopted in this work is to modify the model equations by using experimental data. One of the simplest ways to achieve this isby the regression method. Results of modification by the regression method are shown in Eqs. (23)-(25).

$$a=\frac{p_l}{p_h}-\frac{p_l}{p_h}\theta-\alpha^*\theta-\alpha^*\frac{p_l}{p_h}+\alpha^*\frac{p_l}{p_h}\theta-12\theta \tag{23}$$

$$b=1-\theta-x_f-\frac{p_l}{p_h}+\frac{p_l}{p_h}\theta+\alpha^*\theta+\alpha^*\frac{p_l}{p_h}-\alpha^*\frac{p_l}{p_h}\theta+\alpha^*x_f \tag{24}$$

$$c=-\alpha^*x_f \tag{25}$$

As we can see from Fig. 5, the explicit model exhibits excellent tracking performance in the estimation of recovery. The discrepancy between the results from the model and those from experiments is not large and we can see that the explicit model can be effectively used in the estimation of key variables. To figure out the general trend of changes of purity and recovery, 3-D representations of calculation results based on the neural network model are shown in Fig. 6.

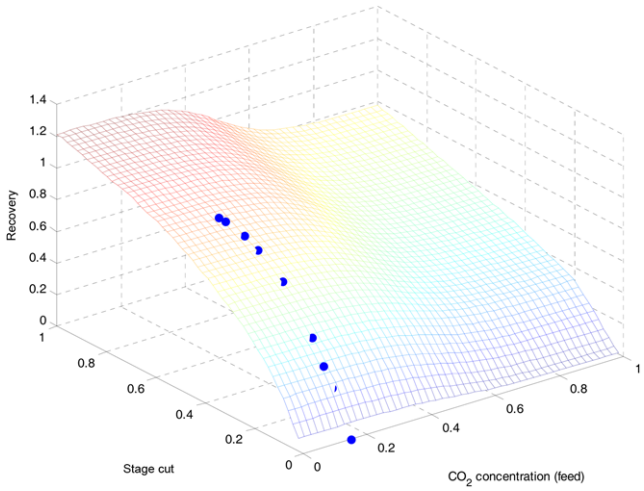

Fig. 6. Estimation results by the MLP neural network model.

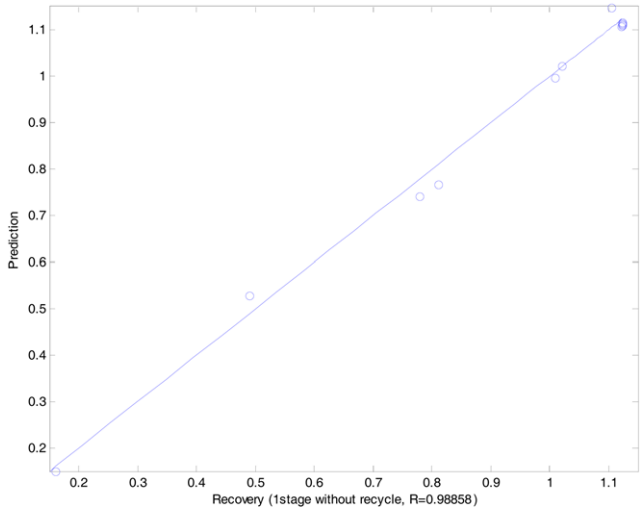

Fig. 7. Predicting performance of recovery for single-stage without recycle (Prediction by MLP model, Recovery by the explicit model).

Figs. 7-10 show predicted performance of recovery for single-stage without (Fig. 7) and with (Fig. 8) recycle as well as for 3-stage without (Fig. 9) and with (Fig. 10) recycle. Simulation conditions are shown in Table 1. In general, values of recovery are less than 1. But we can see that these values exceed 1 in Fig. 8. It seems that accumulation of carbon dioxide within the porous supporting material results in large values of recovery. The reason for the sudden increase or decrease in recovery at specific stage cuts and mole fraction of CO_2 feed is not yet clarified.

In experiments only a single-stage module without recycle was used due to physical constraints. Future experimental plans include multi-stage constructions with recycles. At this time it is inevitable to employ models to investigate effects of recycles as well as multi-

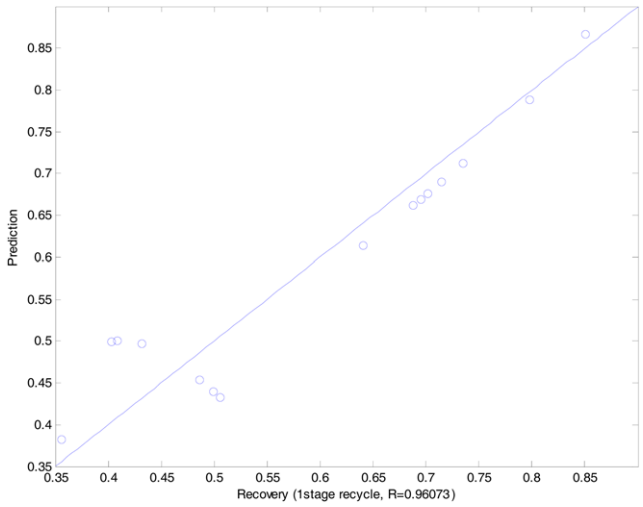

Fig. 8. Predicting performance of recovery for single-stage with recycle (Prediction by MLP model, Recovery by the explicit model).

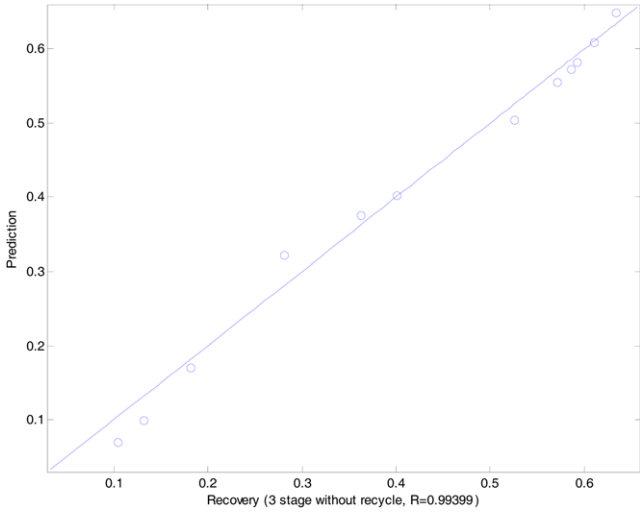

Fig. 9. Predicting performance of recovery for 3-stage without recycle (Prediction by MLP model, Recovery by the explicit model).

stage configurations. The excellent estimating performance of the proposed model displayed in Fig. 5 promises confidential use of the model to examine the effects of recycles and multi-stage configurations. Although the explicit model alone can be used for this purpose, data on recycle operations and multi-stage modules may be provided and neural network models can be effectively used to estimate the effects of key operating variables. Thus it is necessary to establish a methodology for neural network modeling for even more complicated configurations. For this we first generate training data by using explicit models for single and multi-stage modules with and without recycles. These data are used to reconstruct the true underlying surfaces representing the dependency of key variables to stage cuts.

Figs. 7-10 show the predicting performance of the MLP neural network model for single- and multi(three)-stage modules with and

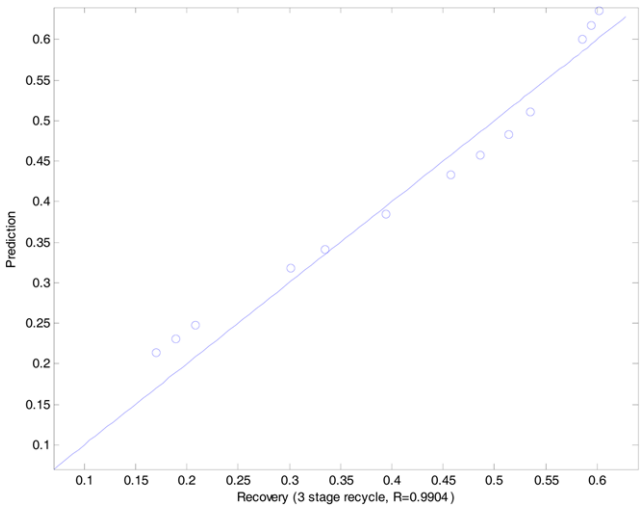

Fig. 10. Predicting performance of recovery for 3-stage with recycle (Prediction by MLP model, Recovery by the explicit model).

without recycles. In these graphs values of the y axis (labeled as "Prediction") are computed by MLP model while those of the x axis (labeled as "Recovery") are computed by the explicit model. Fig. 7 shows the predicting performance of the single-stage module without recycle for recovery. The value of R represents the degree of the match between the MLP neural model and the proposed explicit model. R has a value between 0 and 1, and the closer the value of R to 1, the better the predicting performance of the MLP neural model. Fig. 8 shows the predicting performance of the single-stage module with recycle for recovery. As can be seen, the predicting performance of the recovery by the MLP neural model is little decreased due to the recycle. For the recovery, R is 98.858% without recycle and 96.073% with recycle. In general, the predicting performance is deteriorated by recycle for recovery except the prediction of the recovery for asingle-stage modules. Improvement of the predicting performance by the recycle is more noticeable for 3-stage modules (see Figs. 9-10). Fig. 9 shows the predicting performance of the 3-stage module without recycle for recovery, and Fig. 10 shows the predicting performance of the 3-stage module with recycle for recovery. Again, we can see that the predicting performance is improved by recycle both for recovery for 3-stage module.

CONCLUSIONS

We developed models for the CO_2 separation process by hollow-fiber membrane modules. The explicit model, which is based on mass balances for the separation modules, is compared with the multilayer perceptrons (MLP) back-propagation neural network model. Experimental data obtained from single-stage module without recycle are used to validate the models. The effectiveness of the model is demonstrated by little discrepancy between experimental data and computational results. The explicit model for the single-stage module can easily be extended to the multi(three)-stage module. Because of the lack of experimental data for multi-stage modules, computational data from the explicit model with and without recycle are used as training data set for the MLP neural model. We

could examine the effects of recycle on the recovery based on the results of numerical simulations. We can see that the predicting performance is improved by recycle for multi-stage modules.

ACKNOWLEDGEMENTS

This work was supported by a grant (CDRS II-03-1) from the Carbon Dioxide Reduction & Sequestration Research Center, one of the 21st century frontier programs funded by the Ministry of Science and Technology of Korean Government.

NOMENCLATURE

A_m : effective membrane area [m^2]
q_f : flow rate of the feed side [mol/hr]
q_o : flow rate of the reject side [mol/hr]
q_p : flow rate of the permeate side [mol/hr]
p_h : higher pressure [Pa]
p_l : lower pressure [Pa]
(P_{CO_2}'/t) : specific permeability of species CO_2 through hollow fibers [$mol/m^2 \cdot hr \cdot Pa$]
(P_{N_2}'/t) : specific permeability of species N_2 through hollow fibers [$mol/m^2 \cdot hr \cdot Pa$]
x : local mole fraction of the more permeable component on the feed side [-]
x_f : mole fraction of CO_2 at the feed side [-]
x_o : mole fraction of CO_2 at the reject side [-]
y : local mole fraction of the more permeable component on the permeate side [-]
y_p : mole fraction of CO_2 at the permeate side [-]
α^* : ideal selectivity defined in Eq. (6) [-]
θ : stage-cut defined in Eq. (2) [-]

REFERENCES

1. S. H. Choi, *Theories and Applications of Chem. Eng.*, **14**(1), 298 (2008).
2. H. B. Park, C. H. Jung, Y. M. Lee, A. J. Hill, S. J. Pas, S. T. Mudie, E. V. Wagner, B. D. Freeman and D. J. Cookson, *Science*, **318**, 254 (2007).
3. Y. T. Lee, *Euromembrane*, **200**(1), 169 (2006).
4. N. S. Kim, *Membr. J.*, **17**(4), 318 (2007).
5. B. Noureddine, S. Amltava and S. Kamalesh, *Ind. Eng. Chem. Fundam.*, **25**, 217 (1986).
6. M. J. Thundyil and W. J. Koros, *J. Membr. Sci.*, **125**, 275 (1997).
7. S. H. Choi, J. H. Kim, B. S. Kim and S. B. Lee, *Membr. J.*, **15**(4), 310 (2005).
8. I. H. Song, H. S. Ahn, Y. J. Lee, H. S. Jeon, Y. T. Lee, J. H. Kim and S. B. Lee, *Membr. J.*, **16**(3), 204 (2006).
9. I. H. Song, H. S. Ahn, Y. J. Lee, H. S. Jeon, Y. T. Lee, J. H. Kim and S. B. Lee, *Membr. J.*, **16**(4), 252 (2006).
10. A. Shasav and M. P. Cheuar, *J. Membr. Sci.*, **297**, 59 (2007).
11. R. D. Noble and S. A. Stern, Elsevier Science B.V., 519 (1995).
12. Z. Li and L. Ernst, *J. Membr. Sci.*, **325**, 284 (2008).
13. D. Rumelhar and M. Clelland, *Parallel distributed processing*, Vol.1&2, MIT Press, Boston (1986).
14. T. Kohonen, *Self-Organizing and Associative Memory*, 3rd Ed., Springer-Verlag, Berlin (1989).
15. R. Hecht-Nielsen, *Neurocomputing*, Addison-Wesley, New York (1990).
16. J. J. Hopfield, *Proc. of the National Academy of Sciences*, **79**, 2554 (1982).
17. J. L. Elman, *Cognitive Science*, **14**, 179 (1986).
18. M. I. Jordan, *Proc. of the 8th Annual Conf. of the Cognitive Science Society*, 531 (1986).
19. B. Widrow and M. E. Hoff, *Proc. 1960 IRE WESCON Convention Record*, Part 4:IRE, 96, New York (1960).
20. G. A. Carpenter and S. Grossberg, *Computer*, March 77 (1988).
21. J. H. Hollan, *Adaptation in natural and artificial systems*, University of Michigan Press, Ann Arbor (1975).
22. D. Goldberg, *Generic algorithms in search, optimization and machine learning*, Addison-Wesley, New York (1989).